Catechin encapsulation and controlled release through pH-sensitive multi-branched copolymers for optimized antimicrobial activity

Mohammed Belkadi[1]*, Ridouan El Yousfi[2]*, Oumayma Sayah[3], Mohammed Dalli[4], Aziza Hami[1], and Adil Maleb[5]

ABSTRACT

Conventional delivery systems, such as liposomes or non-responsive micelles, often fail to adequately protect catechin from premature degradation or to achieve effective bioavailability. To address these limitations, we developed an advanced delivery architecture that safeguards catechin and ensures targeted activity within acidic infection microenvironments, offering a promising strategy for antimicrobial therapy amid rising bacterial resistance. In this study, a multi-branched copolymer poly(4-vinylpyridine) (P4VP)-(poly[ε-caprolactone]$_{20}$)$_5$ (PCL) with an AB$_5$ architecture was designed, where P4VP constitutes the hydrophilic segment and PCL forms the hydrophobic segment. This copolymer was engineered to encapsulate catechin and ensure its controlled release. Upon self-assembly in aqueous solution, it formed vesicles with well-defined morphologies, as confirmed by dynamic light scattering and transmission electron microscopy. At physiological conditions (pH 7.0), the vesicles were stable (~90 nm, ζ-potential <3 mV). At acidic conditions (pH 5.5), they underwent structural disorganization accompanied by an increase in size (~130 nm) and surface charge (+42 mV), which triggered catechin release (>90% within 24 h). Antibacterial assays demonstrated a marked enhancement in efficacy after encapsulation. Compared to free catechin, which exhibited limited inhibition zones (7–8 mm), catechin-loaded vesicles achieved zones of 22 mm against *Staphylococcus aureus* and 23 mm against *Escherichia coli*. Minimum inhibitory concentration values also decreased by an order of magnitude, highlighting the superior potency of the encapsulated formulation. Our findings highlight the P4VP-(PCL$_{20}$)$_5$ copolymer as a unique nanocarrier that unifies stability, pH-responsiveness, and drug protection within a single platform.

Keywords:
Nanoencapsulation; Catechin; Controlled release; Self-assembly; Antibacterial activity

***Corresponding authors:**
Mohammed Belkadi,
belkadimedchoukri@gmail.com;
Ridouan El Yousfi,
red1elyousfi@gmail.com

How to cite this article:
Belkadi, M., El Yousfi, R., Sayah, O., Dalli, M., Hami, A., Maleb, A. Catechin encapsulation and controlled release through pH-sensitive multi-branched copolymers for optimized antimicrobial activity. *Biomater Transl.* 2025.
doi: 10.12336/bmt.25.00061

1. Introduction

Bacterial infections pose an increasing threat to global public health, particularly due to the emergence of multidrug-resistant (MDR) strains.[1-3] Among these pathogens, *Staphylococcus aureus* is particularly concerning, ranking as the second most prevalent infectious bacterium after *Escherichia coli*.[4,5] As a Gram-positive pathogen, *S. aureus* is responsible for a wide range of human and animal infections, from superficial skin infections to severe diseases, such as pneumonia, bacteremia, endocarditis, and osteomyelitis, which can lead to fatal complications.[6,7] Its pathogenicity is attributed to its remarkable ability to adapt, allowing it to evade host immune defenses, adhere to host cells, and produce toxins that cause severe tissue damage.[8,9]

The global spread of MDR strains is primarily due to bacterial resistance against previously effective molecules, such as catechin and methicillin.[10] For example, *S. aureus*, as a Gram-positive bacterium, has developed resistance to methicillin.[11] Catechin, a natural polyphenolic compound, exhibits antibacterial activity through multiple mechanisms, including disruption of bacterial membranes, chelation of metal ions, generation of reactive oxygen species, and inhibition of bacterial enzymes essential for cell metabolism

and DNA replication. These mechanisms vary in effectiveness depending on bacterial structure and intrinsic resistance systems, such as efflux pumps.[12] The antibacterial activity of catechins in green tea occurs through several mechanisms, including disrupting cell walls and membranes, inhibiting intracellular enzymes, causing oxidative stress, damaging DNA, and chelating iron.[13] These mechanisms operate simultaneously with relative importance differing among bacterial strains. In all structure-activity relationship studies, the highest antibacterial activity is observed in galloylated compounds (epigallocatechin gallate, epicatechin gallate, and theaflavin digallate). This observation, combined with numerous experimental and theoretical evidences, suggests that catechins share a common binding mode, characterized by the formation of hydrogen bonds and hydrophobic interactions with their target.[13] Despite the use of this active compound in various fields, it suffers from several limitations. For instance, catechin is limited by its poor water solubility and rapid degradation in physiological conditions (particularly at neutral or alkaline pH), significantly reducing its therapeutic efficacy.[14-16] Moreover, uncontrolled diffusion of catechin may lead to non-targeted antimicrobial activity, increasing the risk of cytotoxicity to healthy cells while reducing its effectiveness against specific bacteria.[17-20]

In addition, certain Gram-negative bacteria exhibit relative resistance to catechin, mainly due to the structure of their outer membrane, which limits the permeability of hydrophilic compounds, such as catechins. Studies have shown that clinical strains of *E. coli* and *Pseudomonas aeruginosa* require higher catechin concentrations to inhibit their growth compared to Gram-positive bacteria, such as *S. aureus*.[21,22] Moreover, certain bacteria possess specific defense mechanisms, such as efflux pumps, which actively expel catechins from the cell, thereby reducing the antimicrobial efficacy of catechins. For example, NorA efflux pumps in *S. aureus* are known to decrease the intracellular accumulation of various antimicrobial agents, including catechins.[23] Consequently, although catechin exhibits promising therapeutic potential, its effectiveness may vary depending on the specific characteristics of the target bacteria,[21] including the composition of their cell wall and the presence of intrinsic resistance mechanisms.[24-26] This issue significantly complicates therapeutic strategies, leading to higher morbidity and mortality rates.

Given this critical situation, and to overcome the limitations of natural antimicrobial molecules, such as catechin, various drug delivery strategies have been explored, including liposomes and pH-sensitive polymeric systems, which enhance stability, control release, and target specific cells.[27,28] Liposomes, spherical structures composed of lipid bilayers, can encapsulate both hydrophobic and hydrophilic agents, thereby ensuring controlled release of the active compound. They are stable at physiological pH but destabilize in response to acidic environments, typical of infected tissues, releasing their contents in a targeted manner.[27,28] This approach reduces systemic side effects while enhancing local efficacy. However, their clinical use remains limited due to immune recognition and rapid clearance by the reticuloendothelial system.[27] To improve circulation time and bioavailability, surface modification strategies, such as PEGylation, have been developed, significantly prolonging circulation time and enhancing therapeutic efficacy.[28]

Similarly, pH-sensitive polymers offer a promising alternative. These materials respond to pH variations by altering their structure, resulting in the controlled release of the encapsulated drug. They can swell or shrink depending on the pH, facilitating targeted release in acidic environments typical of infection sites.[29] This property maximizes antimicrobial effects while minimizing impact on surrounding healthy tissues. Moreover, extracellular vesicles (EVs), particularly exosomes, are emerging as innovative drug delivery systems. These natural nanoparticles are biocompatible, capable of crossing biological barriers, and exhibit low immunogenicity, making them particularly suitable for targeted drug delivery.[30] They can be loaded with various therapeutic agents and directed to specific cells, offering a personalized approach to treating bacterial infections. However, large-scale production and functionalization still require further research to optimize their clinical efficacy.[30]

Advances in drug delivery systems—whether liposomes, pH-sensitive polymers, or EVs—represent promising strategies to enhance the effectiveness of antimicrobial treatments. By overcoming challenges related to stability, targeted release, and bioavailability, these technologies offer new perspectives for combating bacterial infections, including antibiotic-resistant strains.

These challenges necessitate the development of optimized drug delivery systems that can protect catechin from degradation, enhancing its bioavailability, and ensuring targeted release at infection sites, thereby maximizing its antibacterial effects while minimizing side effects.[31,32] The encapsulation of catechin in controlled drug delivery systems, such as pH-sensitive polymeric vesicles, represents an innovative strategy to enhance its therapeutic efficacy.[33-35] These polymeric nanostructures not only protect catechin from premature degradation but also enable targeted release in response to specific stimuli, particularly pH variations in infectious microenvironments.[36,37] *S. aureus* infections are often characterized by a locally acidic environment. For instance, *S. aureus* is capable of surviving and proliferating within macrophage phagolysosomes, where the pH is approximately 5.4.[38-40] This local acidity is partly due to the production of

[1]Laboratory of Bioresources, Biotechnology, Ethnopharmacology, and Health, Faculty of Sciences, University Mohammed First, Oujda, Oriental Region, Morocco; [2]Laboratory of Applied Chemistry and Environment, Faculty of Sciences, Mohamed First University, Oujda, Oriental Region, Morocco; [3]Department of Chemistry, Faculty of Sciences, Mohammed First University, Oujda, Oriental Region, Morocco; [4]Department of Human Physiology and Ethnopharmacology, Higher Institute of Nursing Professions and Health Techniques, Mohammed First University, Oujda, Oriental Region, Morocco; [5]Laboratory of Microbiology, Faculty of Medicine and Pharmacy, University Mohammed the First, Oujda, Oriental Region, Morocco

organic acids by bacteria, such as acetic acid, the primary product of glucose catabolism under anaerobic conditions.[41]

The pH-sensitive feature of polymeric vesicles enables the targeted release of catechin at infected sites.[42-45] This approach not only protects catechin from degradation in physiological conditions but also increases its local concentration at the infection site, thereby enhancing its antimicrobial efficacy while minimizing systemic side effects. Studies have shown that encapsulating bioactive compounds in polymeric matrices can enhance their stability and antimicrobial activity.[46,47] For instance, the use of pectin as an encapsulation matrix has demonstrated an enhanced antimicrobial effect of emulsions against foodborne pathogens.[48,49] Similarly, encapsulating catechin in polymeric vesicles could potentially strengthen its activity against *S. aureus*, particularly in acidic environments characteristic of infected sites.[43,50]

In this context, this study presents a solution by developing a multi-branched poly(4-vinylpyridine)-block (P4VP)-poly(ε-caprolactone) $(PCL_{20})_5$ copolymer, which has already been synthesized and characterized in our previous work.[51] Compared to conventional liposomes and single-chain polymers, this copolymer presents an innovative polymeric system designed for pH-responsive catechin delivery, which offers improved stability, targeted release, and enhanced antimicrobial activity compared to conventional systems. Due to its multi-branched structure, P4VP-$(PCL_{20})_5$ self-assembles into stable polymeric vesicles, enabling efficient encapsulation that protects catechin and enhances its bioavailability. The compatibility of P4VP-$(PCL_{20})_5$ with different environments, both polar and apolar, has already been confirmed in our studies.[51] P4VP-$(PCL_{20})_5$ ensures greater application flexibility, allowing for proper dispersion in aqueous solutions while maintaining its integrity in the presence of lipidic or organic phases. Encapsulation within these polymeric vesicles also protects catechin from oxidation and enzymatic degradation in physiological environments, thereby extending catechin's antimicrobial activity until its targeted release.

Furthermore, the pH sensitivity of the P4VP block enables targeted release in acidic environments (pH ~5.5), leading to vesicle disintegration and controlled catechin diffusion at infection sites. This characteristic utilizes the acidic microenvironment of bacterial infections to enhance antimicrobial action. The P4VP block confers sharp pH sensitivity (~5.5), enabling targeted disassembly in acidic microenvironments, such as *S. aureus* infection sites. This targeted release enhances local drug concentration, boosts bactericidal action, and minimizes systemic side effects, offering a promising solution to overcome current delivery barriers. By combining efficient encapsulation, controlled release, and optimized protection, this system increases the local catechin concentration at infection sites, maximizing its bactericidal effect while minimizing systemic side effects.

In this study, the formation and characterization of P4VP-$(PCL_{20})_5$ vesicles were evaluated for their potential as a controlled delivery system for catechin. The self-assembly of the copolymer, catechin encapsulation, and colloidal stability were analyzed as a function of pH. The pH-sensitive properties of the system were investigated by determining the solubility transition (pKb ~5.5), variations in transmittance, vesicle size, and the critical aggregation concentration (CAC). The release kinetics of catechin were evaluated under simulated physiological conditions (pH 7.0 and 5.5), and the mechanism of vesicle disintegration induced by acidification was examined. The antioxidant activity was assessed, and the impact of encapsulation on the stability and duration of action of the active compound was studied to validate the potential of P4VP-$(PCL_{20})_5$ vesicles as an innovative platform for targeted catechin release. Finally, the antimicrobial efficacy of the system was also quantified through tests on various pathogenic strains, allowing a comparison between free and encapsulated catechin.

To further highlight the broader scientific impact and innovative perspectives of this study, the development of pH-responsive P4VP-$(PCL_{20})_5$ vesicles for catechin delivery not only improves the antibacterial efficacy of this specific polyphenol but also provides a versatile platform applicable to other natural bioactive compounds facing similar challenges, such as poor solubility, rapid degradation, or limited bioavailability. This approach could be extended to combat a range of MDR bacterial strains, potentially offering new strategies for addressing critical clinical infections beyond *S. aureus*. Moreover, the successful implementation of these vesicles in controlled drug release systems opens avenues for future clinical applications, including targeted antimicrobial therapy, combination treatments, and personalized medicine approaches, thereby contributing meaningful insights and new perspectives to the field of antimicrobial drug delivery.

This study aims to (i) verify the pH responsiveness of P4VP-$(PCL_{20})_5$ vesicles, (ii) evaluate their capacity to enhance catechin antibacterial activity, (iii) compare this system with existing delivery platforms, such as liposomes and other pH-sensitive polymers, and (iv) elucidate the mechanisms underlying catechin release and bactericidal enhancement in acidic infection environments.

2. Methodology

2.1. Materials

The chemicals used in this study included ε-caprolactone (Sigma-Aldrich, United States of America [USA]), 4-vinyl pyridine (Sigma-Aldrich, USA), hydroxyethyl methacrylate (HEMA; Sigma-Aldrich, USA), 4-cyano-4-([dodecylsulfanylthiocarbonyl] sulfanyl)pentanoic acid (CDPA; Sigma-Aldrich, USA), azobisisobutyronitrile (AIBN; Sigma-Aldrich, USA), tin(II) 2-ethylhexanoate ($Sn[Oct]_2$; Sigma-Aldrich, USA), N,N-dimethylformamide (DMF, American Chemical Society reagent ≥99.8%; Sigma-Aldrich, USA), absolute methanol (≥99.8%; Sigma-Aldrich, USA), dichloromethane (≥99.0%; Sigma-Aldrich, USA), diethyl ether (99.0%; Sigma-Aldrich, USA), and chloroform ($CDCl_3$, ≥99.8%; Sigma-Aldrich, USA).

2.2. Characterization techniques

2.2.1. Nuclear magnetic resonance

Proton nuclear magnetic resonance (^{1}H NMR) spectroscopy was performed at a frequency of 500 MHz using a spectrometer

(Avance, Bruker Corporation, USA). Depending on the solubility and nature of the sample, deuterated solvents, such as $CDCl_3$, dimethyl sulfoxide, or water, were employed. The samples were prepared at a concentration of approximately 25 mg/mL and analyzed at room temperature in 5 mm NMR tubes.

2.2.2. Attenuated total reflectance-Fourier transform infrared spectroscopy

Infrared spectra were recorded using a Fourier transform infrared spectrometer (FTIR; FT/IR-4700, Jasco International Co., Ltd., Japan) equipped with an attenuated total reflectance accessory. The spectral acquisition range extended from 400 to 4,000 cm^{-1}. For each sample, 32 scans were averaged at a resolution of 4 cm^{-1}. A background spectrum was collected before each measurement to ensure signal accuracy and consistency.

2.2.3. Transmission electron microscopy (TEM)

TEM analyses were performed at 200 kV using a microscope (Talos F200S, Thermo Fisher Scientific, USA), which offered a resolution of 0.12 nm in imaging mode. Images were captured using a 4,096 × 4,096 pixel camera (Ceta™ 16M, Thermo Fisher Scientific, USA), and elemental analysis was enabled through an energy-dispersive X-ray detector (Super-X, Thermo Fisher Scientific, USA) with a 136 eV resolution. For sample preparation, a 20 μL droplet of polymer solution (0.1 mg/mL) was deposited on a carbon-coated copper grid and left for 2 min. Excess fluid was blotted off, followed by staining with 20 μL of 2 mg/mL uranyl acetate to provide negative contrast around the structures of interest. After a brief exposure, excess stain was removed, and the grid was allowed to air dry.

2.2.4. Turbidity measurements

Turbidity was assessed by measuring light transmittance through the samples using a particle characterization instrument (Litesizer™ 500, Anton Paar GmbH, Austria), which operates over a temperature range of 0–90°C. In the case of polyethylene glycol (PEG)-PCL solutions, measurements were temperature-dependent, necessitating an equilibration period before data collection. Typically, a 2-min equilibration time was used near room temperature. For temperatures ranging from 30°C to 45°C, additional equilibration time was added (approximately 1 min per °C above room temperature) for 1 mL sample volumes.

2.2.5. Dynamic light scattering (DLS)

The hydrodynamic diameter of copolymer assemblies in aqueous solution (0.1 wt%) was determined using DLS with the same instrument used for turbidity measurements. The instrument utilizes a 658 nm laser diode (40 mW) and allows measurements across a range of scattering angles (15–175°). At each temperature point, the sample was equilibrated for 30 min. The obtained correlation functions were used to extract diffusion coefficients, from which particle sizes were calculated using the Stokes–Einstein equation.

2.2.6. Static light scattering

Static light scattering experiments were conducted at a fixed angle of 90° using the same instrument as DLS to estimate the molar mass of the polymers. Scattering intensity was recorded at varying concentrations to construct Debye plots, from which the intercept yielded the molecular weight. Measurements were performed in water at concentrations below the CAC to analyze the polymer in its unassociated form. Toluene was used as the calibration standard, and the solvent background was subtracted from all measurements.

2.3. Synthesis of multi-branched copolymers with poly(4-vinylpyridine) and hydroxyethyl methacrylate-poly(ε-caprolactone)

A multi-branched copolymer with an AB_5 topology, P4VP-$(PCL_{20})_5$, was synthesized, where A represents the P4VP block, B the PCL block, and 5 the number of PCL arms, corresponding to the degree of polymerization (DP) of HEMA–PCL_{20}. This synthesis involved three essential steps: (i) preparation of a pre-macro-monomer based on HEMA–PCL_{20} with a chain length of 20 units; (ii) synthesis of a reversible addition–fragmentation chain transfer (RAFT) macro-agent derived from P4VP-chain transfer agent (CTA); and (iii) RAFT polymerization of HEMA–PCL_{20} macromonomers using P4VP-CTA, yielding the final multi-branched copolymer structure.

This strategy builds on our recent work reporting the production of precise and regulated polymeric structures.[52] A key advantage of the AB_X multi-branched copolymer design lies in its structural tunability: the number of PCL arms can be varied to modulate the mechanical, chemical, and physical characteristics of the material. This degree of control enables applications across polymer chemistry, advanced materials, and nanotechnology.

2.3.1. Synthesis of polyvinyl pyridine macro-reversible addition-fragmentation chain transfer polymerization agent

Using CDPA as the RAFT agent, P4VP-CTA was synthesized by RAFT polymerization in solution with a DP of 50 (**Figure 1**). Following established procedures,[52] the synthesis was carried out in bulk. In short, a dry polymerization tube was filled with 4-vinylpyridine (4VP; 5 g, 47.6 mmol), CDPA (0.34 g, 0.93 mmol), and AIBN (16.0 mg, 0.01 mmol). After 30 min of nitrogen purging at room temperature, the mixture was submerged for 4 h in an oil bath that had been preheated to 80°C. Tetrahydrofuran (THF) (1 mL) was added after polymerization, and the crude product was purified by running it through a silica column. The polymer was precipitated into toluene, filtered, and then vacuum-dried for 24 h at room temperature to eliminate the unreacted 4VP monomer. A pink powder (0.73 g, 75% yield) was the final form of P4VP-CTA. ^1H NMR in $CDCl_3$ was used to determine the number-average molecular weight (Mn) and the number-average DP, which reported values of 5,299 and 49 $gmol^{-1}$, respectively.

2.3.2. Preparation of hydroxyethyl methacrylate-poly(ε-caprolactone)20 macro-monomer

Using HEMA as the initiator, ring-opening polymerization of ε-caprolactone was used to create HEMA-PCL_n

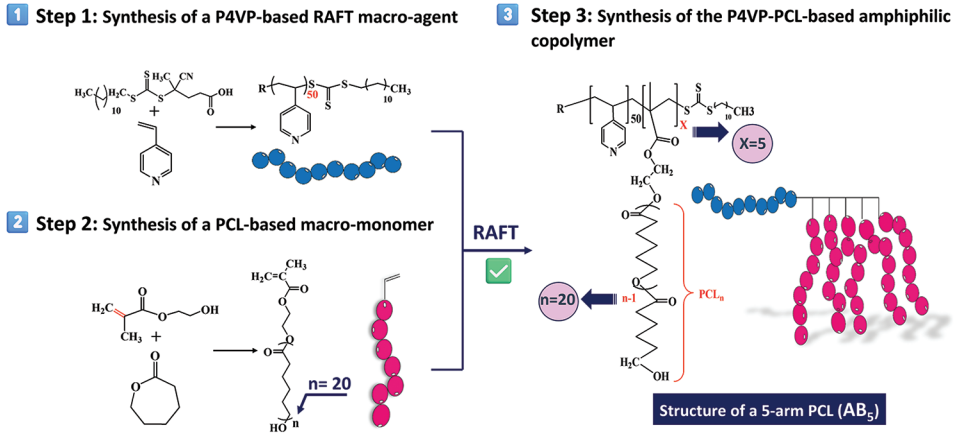

Figure 1. Synthetic pathway for the amphiphilic copolymer P4VP-$(PCL_{20})_5$ through RAFT polymerization
Abbreviations: P4VP: Poly(4-vinylpyridine); P4VP-$(PCL_{20})_5$: Poly(4-vinylpyridine)-(poly[ε-caprolactone]$_{20})_5$; PCL: Poly(ε-caprolactone); RAFT: Reversible addition-fragmentation chain transfer polymerization.

homopolymers with a chain length of n = 20. The bulk polymerization was performed in a glass flask at 120°C for 12 h in a nitrogen atmosphere by vigorously stirring a mixture of HEMA (228 µL), ε-caprolactone (4 mL), and the catalyst, $Sn(Oct)_2$ (16 mg). The crude product was allowed to cool to room temperature before being dissolved in chloroform and precipitated in excess diethyl ether. The product was further purified by dissolving it in dichloromethane and precipitating it once more in excess methanol to guarantee the elimination of any remaining HEMA monomer.

Before use, the finished HEMA–PCL_{20} product was stored at 4°C after being vacuum-dried for 4 h. A lengthy PCL chain connected to a methacrylate group contributed to this macro-monomer, allowing for its subsequent polymerization under RAFT polymerization conditions.

2.3.3. Development of the poly(4-vinylpyridine)-(poly[ε-caprolactone]$_{20})_5$ multi-branched copolymer topology

Hydroxyethyl methacrylate-PCL_n (0.5 g) and 1 g of P4VP-CTA (macro-RAFT agent) (0.17 mmol) were added to a polymerization tube (**Table 1**) along with AIBN (5 mg, 0.017 mmol) and DMF (1 mL) to create the multi-branched copolymer by sequential RAFT polymerization in solution. Before nitrogen bubbling and a continuous stream of nitrogen over the reaction medium throughout the reaction, the solution is first degassed with nitrogen at 0°C for 30 min. After that, the polymerization tube was submerged in a preheated oil bath at 80°C for 4 h. To halt the polymerization, the flask was quickly cooled by submerging it in ice water. DMF and anhydrous ether were then used to dissolve and precipitate the residue multiple times to ensure complete removal of unreacted materials. The resultant orange to pale yellow powder was vacuum-dried for two days at 40°C.

2.3.4. Encapsulation of catechin in poly(4-vinylpyridine)-(poly[ε-caprolactone]$_{20})_5$ vesicles

In this study, multilayer vesicles were prepared from the amphiphilic copolymer P4VP-$(PCL_{20})_5$, where P4VP forms both the interior and exterior of the vesicle, while the intermediate membrane is made of PCL. The catechin was encapsulated in the internal cavity of the vesicle. The P4VP-$(PCL_{20})_5$ copolymer is first dissolved in THF at a concentration of 25 mg/mL under magnetic stirring at room temperature. Meanwhile, 10 mg of catechin is dissolved in 1 mL of ethanol under moderate stirring for 15 min to ensure homogeneous solubilization. The catechin solution is then gradually added to the polymer solution under constant stirring for 30 min to promote optimal interaction between the catechin and the copolymer. The self-assembly of the vesicles is induced by the controlled dropwise addition of ultrapure water (5 mL/h) under stirring at 500 rpm. A mild sonication is performed at 40% power for 5 min. After the vesicles are formed, the organic solvents (THF, ethanol) are removed by evaporation under vacuum using a rotary evaporator, maintained at a temperature of 40°C and a pressure of 150 mbar to prevent any degradation of the encapsulated components. The suspension is then dialyzed against ultrapure water using a dialysis membrane (Molecular weight cutoff = 10 kDa) for 24 h. This allows the removal of residual solvents, resulting in purified and stable vesicles with optimal hydration balance.

This mechanism enables the selective precipitation of PCL, which assembles into an intermediate membrane, while P4VP positions itself at the inner and outer interfaces of the vesicle.[53,54]

2.4. Characterization of vesicles and profiling of controlled release

The vesicles were characterized using DLS to assess their particle size and colloidal stability. TEM was employed to visualize and confirm their multilamellar structure. The encapsulation efficiency (EE) of catechin was determined using ultraviolet (UV)-visible light (Vis) spectroscopy. To evaluate the pH-responsive release behavior, the vesicles were incubated in two different buffer systems: a physiological buffer at pH 7.0 (simulating healthy tissue) and an acidic buffer at pH 5.5 (mimicking an infected environment). The amount of catechin released was monitored at specific time intervals (0, 2, 4, 8, and 24 h) using UV-Vis analysis. A slow-release profile was expected under neutral conditions (<10% release

Table 1. Antibacterial activity of pH-responsive P4VP-$(PCL_{20})_5$ vesicles

Samples (R ratio)	Catechin concentration	pH	Inhibition zone in mm				
			Escherichia coli (Gram –)	*Salmonella enterica* (Gram –)	*Pseudomonas aeruginosa* (Gram –)	*Listeria monocytogenes* (Gram +)	*Staphylococcus aureus* (Gram +)
Free cat	50 mg/mL	7.0	7.0±0.02	ND	ND	8.0±0.01	7.0±0.01
Blank vesicles	-	5.5	8.0±0.02	9.0±0.1	7.0±0.2	8.0±0.01	7.0±0.03
Cat-polymer (0.4)	200 μg/mL	7.0	11.0±0.2	ND	7.0±0.2	7.0±0.2	10.0±0.2
Cat-polymer (0.6)	300 μg/mL		13.0±0.3	09.0±0.3	09.0±0.3	10.0±0.3	12.0±0.3
Cat-polymer (0.4)	200 μg/mL	5.5	18.0±0.2	16.0±0.2	17.0±0.2	16.0±0.2	19.0±0.2
Cat-polymer (0.6)	300 μg/mL		23.0±0.3	20.0±0.3	20.0±0.3	21.0±0.3	22.0±0.3
T+	-	7.0	22.0±0.1	19.0±0.1	20.0±0.1	20.0±0.1	20.0±0.1

Abbreviations: Cat: Catechin; ND: Not detected; P4VP-$(PCL_{20})_5$: Poly (4-vinylpyridine)$_{50}$-(poly[ε-caprolactone]$_{20}$)$_5$; T: Gentamicin.

over 24 h), while a significantly faster release was anticipated in acidic medium (>50% within 4 h and over 90% after 24 h), demonstrating the system's potential for targeted drug delivery to infection sites.

This approach provides a robust platform for producing stable and functional vesicles that can selectively release catechin in acidic environments, highlighting their potential for biomedical applications, such as antibacterial therapies and wound healing.

2.5. 2,2-diphenyl-1-picrylhydrazyl (DPPH) test

The methodology was adapted here with slight modifications to evaluate the DPPH free-radical scavenging ability of the essential oils at λ_{max} (517 nm). DPPH is a stable and highly colored free radical soluble in methanol, capable of abstracting labile hydrogen atoms from phenolic antioxidants, leading to the concomitant formation of a yellow hydrazine DPPH–H. A freshly prepared solution of DPPH in methanol (4 mg/100 mL) was used, and 0.5 mL of this solution was added to 0.5 mL of essential oil solution in methanol at various concentrations (200, 400, 600, 800, and 1,000 μg/mL). After agitation, the mixture was incubated for 30 min in the dark at room temperature. The absorbance was then measured at 517 nm using a UV-Vis spectrophotometer after correction with a blank (a mixture without essential oil). The same procedure was followed for the positive control: ascorbic acid. The absorbance of the control reaction and the samples was measured, and the percentage of DPPH free radical inhibition, I%, was calculated using Equation 1.[55]

$$I\% = \frac{A_C - A_S}{A_C} \times 100\% \quad (1)$$

Where A_C is the absorbance of the control reaction (containing all reagents except the test sample), and A_S is the absorbance of the test sample. All tests were performed in triplicate, and the curve was plotted using the average value.

2.6. Antibacterial activity of catechin encapsulated in pH-responsive poly(4-vinylpyridine)-(poly[ε-caprolactone]$_{20}$)$_5$ vesicles

The antibacterial activity was evaluated against a panel of bacterial strains, including two Gram-positive species. Antimicrobial susceptibility was assessed using the agar diffusion method on Mueller–Hinton agar. Before inoculation, bacterial suspensions were adjusted to a concentration of 10^6 CFU/mL by measuring optical density at 600 nm with a UV-visible spectrophotometer. The inoculated plates were incubated at 37°C for 24 h. This experimental design aimed to determine the inhibitory potential of the tested samples against both Gram-positive and Gram-negative bacterial pathogens.

3. Results and discussion

3.1. Structural and morphological insights into synthesized copolymers: Composition, architecture, and analysis

Figure 2A displays the FTIR spectrum of P4VP-CTA. The characteristic stretching vibrations of the C=N and C=C bonds in the pyridine ring are observed at approximately 1,599–1,557 cm^{-1} and 1,450–1,415 cm^{-1}, respectively. Absorption bands at 2,940 and 3,023 cm^{-1} are attributed to the aromatic CH_2 stretching vibrations present in the homopolymer.[56]

The synthesized HEMA–PCL_n macro-monomers were analyzed by FTIR spectroscopy. The spectrum shown corresponds to HEMA-PCL_n. A distinct stretching vibration band of the ester carbonyl group (C=O) is detected at 1,722 cm^{-1}, characteristic of the PCL moiety, while a broad band at 3,430 cm^{-1} is assigned to the hydroxyl (–OH) group.[57]

Figure 2B shows the macro-RAFT agent P4VP-CTA's typical ^{1}H NMR spectrum. The successful polymerization of 4VP is confirmed by the appearance of pyridine proton signals at δ = 8.30 ppm and 6.35 ppm and the disappearance of the vinyl proton signals of 4VP at δ = 5.45–5.55 ppm. Proton signals from the RAFT agent moiety (δ = 1.25 ppm) and the P4VP-CTA backbone (δ = 8.0–8.5 ppm) were integrated.[58] The P4VP block's DP was found to be roughly 49 units, which is quite close to the desired DP of 50 units. A number-average molecular weight (M_n) of 5,551.86 $gmol^{-1}$ was obtained from quantitative ^{1}H NMR analysis of the macro-agent, which closely matched the theoretical value (M_n = 5,657 $gmol^{-1}$).

Figure 2C displays the synthesized HEMA-PCL_n macro-monomer's ^{1}H NMR spectrum. The methylene protons (–CH_2–OH) at the chain end of the PCL segment are represented by the triplet at δ = 3.6 ppm (peak g). The terminal HEMA group's distinctive olefinic proton signals are detected at δ = 5.5–5.7 ppm and δ = 6.0–6.7 ppm. At δ = 1.3, 1.6, 4.0, and

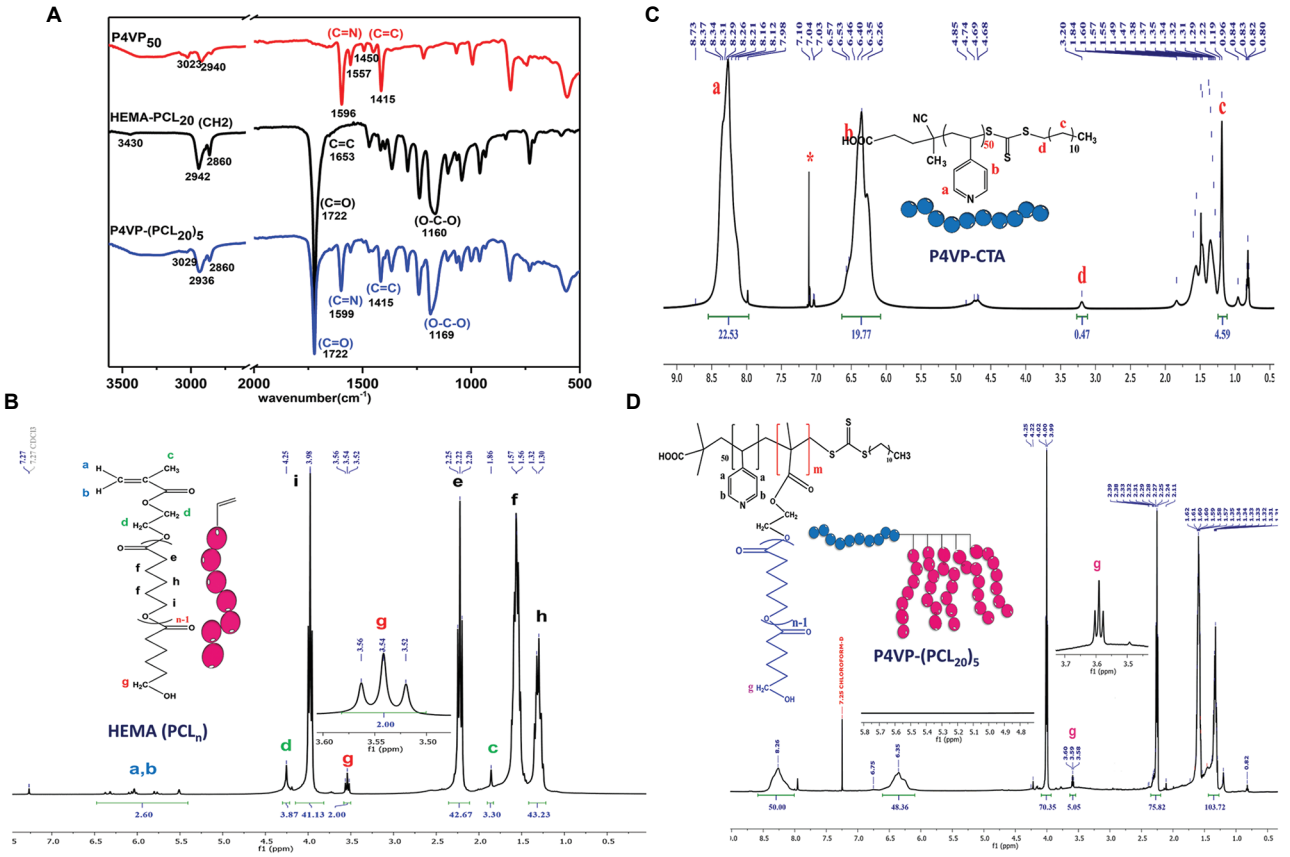

Figure 2. Analysis of the production of P4VP-$(PCL_{20})_5$. (A) FTIR spectra of $P4VP_{50}$, HEMA–PCL_{20}, and the final copolymer P4VP-$(PCL_{20})_5$. (B) ^{1}H NMR spectrum of the RAFT-synthesized $P4VP_{50}$ macro-agent (P4VP-CTA). (C) ^{1}H NMR spectrum of the 5-arm HEMA–PCL_{20} macro-monomer. (D) ^{1}H NMR spectrum of the final amphiphilic copolymer P4VP-$(PCL_{20})_5$.
Abbreviations: CTA: Chain transfer agent; FTIR: Fourier transform infrared spectrometer; HEMA: Hydroxyethyl methacrylate; NMR: Nuclear magnetic resonance; P4VP: Poly(4-vinylpyridine); P4VP-$(PCL_{20})_5$: Poly(4-vinylpyridine)-(poly[ε-caprolactone]$_{20}$)$_5$; PCL: Poly(ε-caprolactone); RAFT: Reversible addition-fragmentation chain transfer polymerization.

4.2 ppm, signals that correspond to the PCL chain's repeating units (–O–CH_2–$(CH_2)_3$–CH_2–CO–) are visible.[59]

End-group analysis was conducted to ascertain the extent of PCL block polymerization in the macro-monomer. A DP_n of 20.5 was obtained by calculating the integration ratio of peaks i and g. A strong correlation between the experimental and theoretical values for every macro-monomer confirmed the accuracy of the synthesis. The agreement between theoretical and NMR-derived DP_n and M_n indicated an excellent control over the chain length of HEMA–PCL_n.

Figure 2D shows the typical ^{1}H NMR spectrum of AB_5-type copolymers, whose importance will be further explored in relation to self-assembly. In the case of the synthesized P4VP-b-$(HEMA–PCL_n)_X$ copolymers, n represents the length of each PCL arm, and X indicates the number of PCL arms connected to the P4VP core. The meta and ortho protons of the pyridine rings are represented by the two broad signals seen at δ = 8.15–8.6 ppm and δ = 6.27–7.07 ppm, respectively.

In addition, a signal at δ = 4.2 ppm is assigned to the methylene protons (-O-CH_2-) within the PCL chains, while the peak at δ = 3.6 ppm corresponds to the –CH_2–OH terminal protons. By comparing the vinyl proton signals of the HEMA–PCL monomer (δ = 5.32–5.57 ppm) with the backbone protons of P4VP-CTA (δ = 0.78–0.84 ppm), the conversion of the HEMA–PCL_n macro-monomer in different copolymers was ascertained using Equation 2.

$$Conversion\% = 1 - \frac{6I_{5.32-5.57}}{2I_{0.78-0.84}} \quad (2)$$

The equation can be used to determine the theoretical M_n ($M_{n,th}$) of each polymer type based on its final conversion (Equation 3).

$$M_{n,th} = \frac{(HEMA - PCL_n) \times M_{HEMA-PCLn}}{(P4VP - TCC)} \times Conversion + M_{P4VP-CTA} \quad (3)$$

However, another intriguing parameter that must be found in all kinds of structures is the DP of the macro monomer HEMA-PCL_n. For this reason, the integrals corresponding to the methylene proton (–CH_2–OH) at the end of the chain PCL were used to validate the DP value and demonstrate the number of arms of PCL connected to the chain P4VP (Equation 4):

$$DP = \frac{I_{3.6}}{I_{8.0-8.5}} DP_{P4VP-CTA} \quad (4)$$

In this instance, Equation 5 was used to determine the experimental molecular masses.

$$M_{n,th} = (M_{HEMA\text{-}PCLn} \times DP) + M_{P4VP\text{-}CTA} \quad (5)$$

The NMR structural analysis revealed that the targeted PCL arms' DP was well-controlled, resulting in the desired topologies. The copolymers' identical masses were confirmed by the molar mass results, enabling us to investigate how topology affects the physical properties of the copolymers with identical molar masses. In addition, all of the RAFT-induced copolymerizations were well-controlled, and the resultant copolymers displayed low dispersity and expected molecular weights.

3.2. Characterization of the pH-responsive polymer segment

The study of the pH sensitivity of the P4VP-$(PCL_{20})_5$ copolymer was conducted by analyzing three parameters: the pH variation as a function of the volume of added sodium hydroxide (NaOH), transmittance (%), and zeta potential (ζ) (**Figure 3**). The obtained results highlight the pH-responsive behavior of the copolymer, characterized by a solubility transition occurring around an estimated pK_b of 5.5.

The evolution of pH with NaOH addition exhibited a three-step variation. Upon the initial introduction of NaOH, the pH increased rapidly before reaching a plateau between 5.0 and 5.5. This stabilization phase was attributed to the gradual ionization of the tertiary amine groups in P4VP.[60,61] With further addition of NaOH, the pH resumed its rapid increase, indicating the completion of amine group neutralization. These findings confirmed that the copolymer's pH-sensitive range lies between 5.0 and 5.5 and that the pK_b value was approximately 5.2, corresponding to 50% neutralization of the tertiary amine groups in the 4VP cycle. Transmittance analysis revealed a significant change in the copolymer's solubility state. At acidic pH between 3.0 and 5.0, the solution was transparent with a transmittance of 98%, indicating complete copolymer solubility. As pH approaches 5.5, a rapid decrease in transmittance to approximately 50% was observed, indicating an increase in turbidity due to the formation of colloidal aggregates. Finally, above pH 5.5, transmittance dropped drastically to around 1%, indicating complete precipitation of the copolymer and opacification of the solution. The changes in the zeta potential explain these solubility transitions. Under acidic conditions (pH < 5.5), the tertiary amine groups of P4VP were protonated, resulting in the copolymers with a high positive charge and a zeta potential of over +30 mV. When pH reached 5.5, the zeta potential gradually decreased to a value between +2 mV and 0 mV, reflecting charge neutralization and the loss of hydrophilic interactions, which led to aggregate coalescence. Finally, at pH >5.5, the zeta potential became negative, reflecting the complete deprotonation of P4VP tertiary amines.[62,63]

These results confirm the pH-sensitive properties of P4VP-$(PCL_{20})_5$ copolymers, indicating a marked transition ranging from pH 5.0–5.5. These observations demonstrate the potential

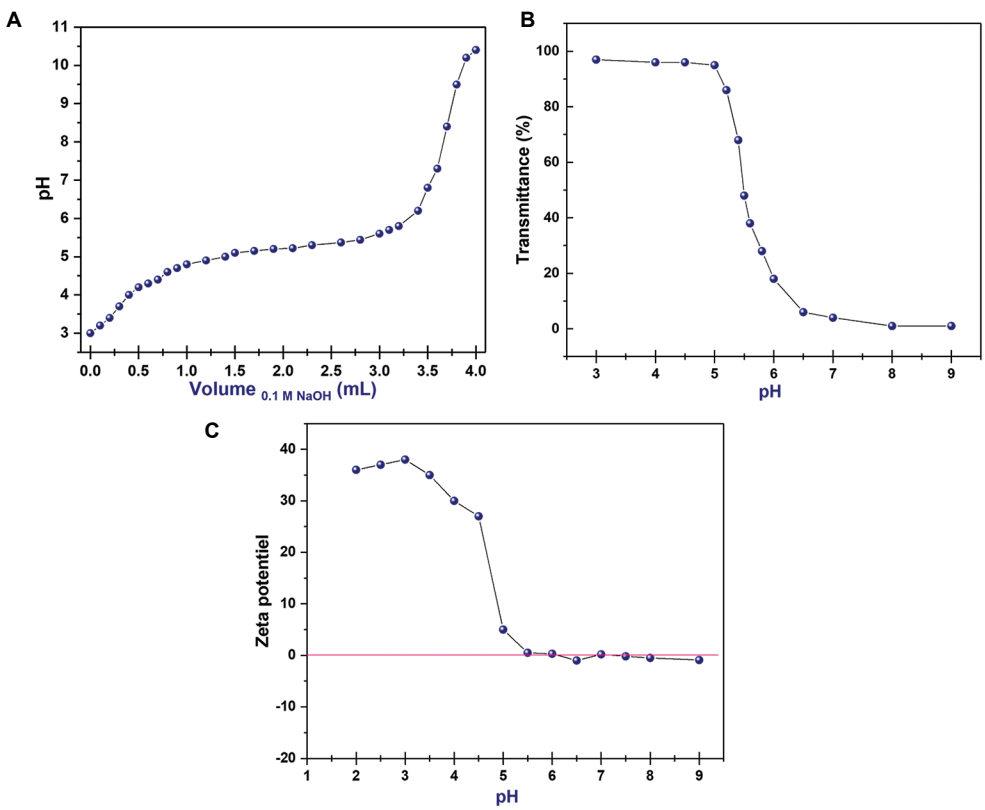

Figure 3. pH-sensitivity and aggregation behavior of P4VP-$(PCL_{20})_5$ copolymer. (A) Evolution of pH as a function of NaOH (0.1 M) volume. (B) Transmittance variation (%) as a function of pH. (C) Zeta potential (ζ) variation as a function of pH. Abbreviations: NaOH: Sodium hydroxide; P4VP-$(PCL_{20})_5$: Poly(4-vinylpyridine)-(poly[ε-caprolactone]$_{20}$)$_5$

of using pH as a trigger for the copolymers, paving the way for intelligent targeted delivery systems.[64,65]

3.3. CAC

The CAC of the P4VP-$(PCL_{20})_5$ polymer at different pH values (7.5 and 5.5) highlights the influence of pH on aggregate formation. The determination of this critical concentration was explored using a method validated in one of our recent works.[51,52] This method relies on correlating the results of three parameters: light transmitted, light scattered, and the size of aggregation. The CAC is defined as the point at which there is an abrupt decrease in transmittance and an instantaneous rise in aggregate size and light scattering intensity.[52] The CAC is recorded at this critical point when micelle or vesicle formation begins. The results presented in **Figure 4A** and **B** show that the CAC values for P4VP-$(PCL_{20})_5$ were 6.92 mg/L at pH 7.0 and 15.14 mg/L at pH 5.5, highlighting the impact of pH on aggregate formation. At pH 7.0, the 4VP segments were minimally protonated,[66] promoting effective vesicle stabilization due to a balance between the hydrophobic and hydrophilic regions of the copolymer. In contrast, at pH 5.5, the increased protonation of amine groups increased the hydrophilicity of 4VP segments,[67] which increased the repulsive forces between the long chains. This hindered vesicle formation, thus increasing the CAC. The variation in CAC with pH underscores the influence of protonation on the copolymer's structure and the formation of aggregated structures.

3.4. Characterization of catechin-loaded vesicles

The properties of empty and catechin-loaded vesicles were examined. The results obtained are presented in **Figure 5** and **Table 2**. As expected, the DLS analyses in **Figure 5F** show that the copolymer particle size remains virtually unchanged (around 85–90 nm) as the pH decreases from 9.0 to 7.0. This is due to the weakly protonated P4VP chains that result in compressed and isolated vesicle structures. However, as pH decreased further (between 7.0 and 5.5), vesicle size increased considerably, from 90 nm to 130 nm. This phenomenon is attributed to the complete protonation of the tertiary amine groups in the 4VP ring of the main chain, resulting in a transformation from hydrophobic to hydrophilic, which caused the structure to be relaxed and swollen. At pH below 5.5, complete protonation of the amine groups resulted in a maximum transformation of the hydrophobic domains of P4VP into hydrophilic ones. This modification promoted water uptake within the vesicles, leading to increased surface tension and potentially causing the structures to disintegrate. However, a plateau in size is observed, indicating that the vesicles reached a limit of swelling with stabilized size.

Regarding the zeta potential, **Figure 5E** shows that the zeta potentials of empty and catechin-loaded vesicles are almost null at pH 7. As the pH decreased from 9.0 to 7.0, the zeta potential remained virtually unchanged (<1 mV). However, as the pH continued to fall, the zeta potential rose rapidly (approximately +32 mV), which was attributed to the complete protonation of 4VP. In addition, this strong positive charge caused increased repulsive forces between the stretched hydrophilic chains, leading to an increase in particle size.

The results also suggested an optimum pH for drug loading at 7.0 to achieve high EE. As the initial amount of catechin increased, the loading capacity (LC) and EE also increased. The actual levels of catechin loading in the polymer were 10.2%, 35.6%, and 52.3% respectively, depending on the different catechin/polymer ratios. On the other hand, when the catechin/polymer ratio was 15 mg/25 mg, EE reached its maximum (87.6%). On the other hand, when this ratio reached 20 mg/25 mg, the LC was slightly higher, but EE decreased slightly due to the limited space for catechin loading.

Catechin-loaded aggregates were slightly larger in size than empty vesicles, reflecting the encapsulation of catechin in

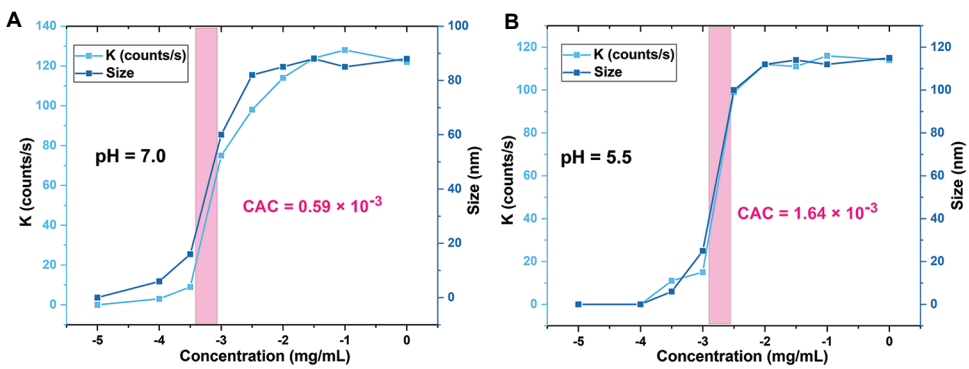

Figure 4. Critical aggregation concentration of P4VP-$(PCL_{20})_5$: Poly(4-vinylpyridine)-(poly[ε-caprolactone]$_{20}$)$_5$. (A) pH = 5.5. (B) pH = 7.0.

Table 2. Characteristic properties of cat-loaded P4VP-$(PCL_{20})_5$

R ratio of cat-polymer	Polymer (mg)	Cat (mg)	Cat: polymer ratio	LC (%)	EE (%)	Particle size (nm)	PDI	Zeta potential (mV)
0.4	25	10	0.4	10.2	62.1	97	0.152	2.2
0.6	25	15	0.6	35.6	87.6	108	0.117	1.3
0.8	25	20	0.8	52.3	73.0	123	0.162	6.3

Abbreviations: Cat: Catechin; EE: Encapsulation efficiency; LC: Loading capacity; P4VP-$(PCL_{20})_5$: Poly (4-vinylpyridine)-(poly[ε-caprolactone]$_{20}$)$_5$; PDI: Polydispersity index.

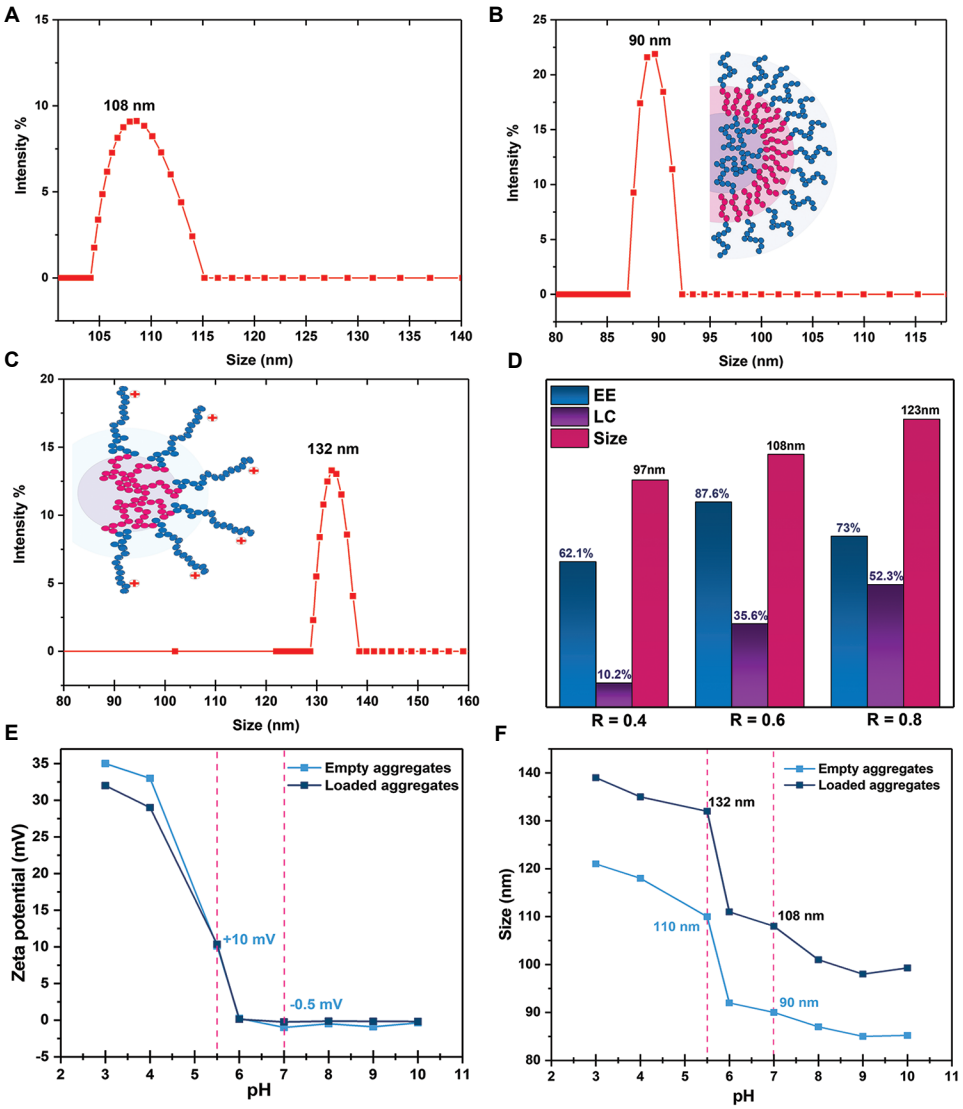

Figure 5. Characterization of catechin-loaded vesicles. (A) Size distribution of nanoaggregates determined by DLS for catechin-loaded vesicles at R = 0.6 and pH = 7 (108 nm). (B) Size distribution of empty vesicles at pH = 7. (C) Size distribution of catechin-loaded vesicles at R = 0.6 and pH = 5.5 (132 nm). (D) EE, LC, and average hydrodynamic size as a function of the R ratio. (E) Zeta potential of empty and loaded nanoaggregates as a function of pH. (F) pH-responsiveness of aggregate size for both empty and loaded vesicles.
Abbreviations: EE: Encapsulation efficiency; LC: Loading capacity.

the vesicle core as well as its adsorption to the vesicle surface. Other characteristic properties are shown in **Table 2**.

3.5. TEM and pH-sensitivity analysis of the vesicles

Figure 6 shows TEM images of vesicles in buffer solutions (PBS, pH 7.0 and 5.5). The results highlight the sensitivity of vesicles to pH variations, a key parameter for applications in controlled drug delivery. In particular, this property could be exploited to release the active ingredient in acidic environments.

Image analysis reveals that the nanoparticles adopt a vesicle-like morphology, with a size of around 92 nm. This observation confirms the ability of the copolymers to self-organize into vesicles under physiological conditions, aligned with a previous study.[52] The influence of pH on these vesicles is a determining factor in their stability and structure. The presence of tertiary amino groups derived from 4VP contributes to the pH-sensitivity of the vesicles, due to their ability to protonate or deprotonate depending on the surrounding environment. At neutral conditions (pH 7.0), vesicles have a well-defined, homogeneous structure, reflecting a balance between hydrophobic and hydrophilic interactions. As pH decreases, the progressive protonation of the amine groups in 4VP leads to an increase in the positive charge of the vesicles.[68] This induces increased electrostatic repulsion between the polymer chains, leading to membrane expansion and vesicle swelling. This transition resulted in a significant increase in vesicle diameter, from 90 nm to 130 nm, which was confirmed by DLS analysis. TEM imaging (**Figure 6**), combined with zeta potential and DLS measurements, was used to analyze the behavior of the vesicles as a function of pH. Zeta potential monitoring confirmed the increase in the positive charge of

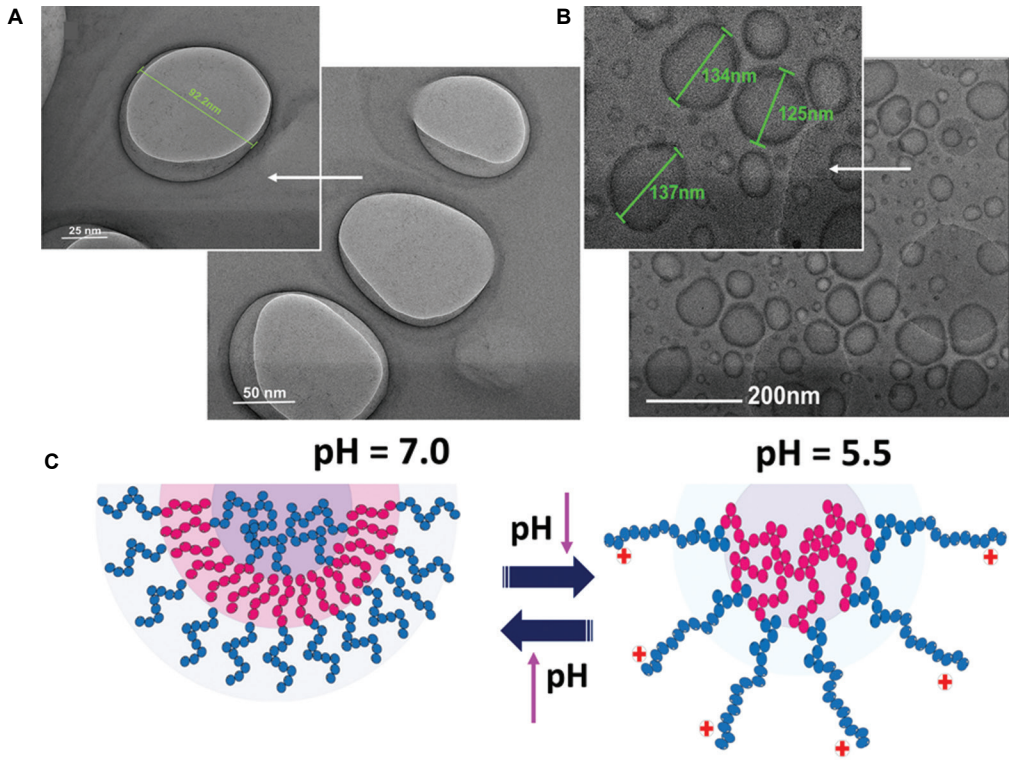

Figure 6. Transmission electron micrographs and schematic representation of P4VP-$(PCL_{20})_5$ vesicles at different pH values. (A) Stable vesicles with well-defined bilayer structure at pH 7.0 (membrane thickness ≈ 8.2 nm). Left: Scale bar: 50 nm; Right: scale bar: 25 nm; magnification: ×15,000. (B) Enlarged and destabilized vesicles at pH 5.5 (diameter ≈ 125–137 nm) due to protonation of P4VP units. Scale bar: 200 nm; magnification: ×12,000. (C) Schematic illustration of the pH-responsive mechanism: Compact bilayer at neutral pH versus swollen and disorganized structure under acidic conditions.

vesicles at acidic pH, explaining their tendency to swell. In addition, DLS analysis validated the size distribution observed in TEM, confirming the structural transition induced by protonation of the amine groups.

3.6. *In vitro* release of catechin

The *in vitro* release profile of catechin from P4VP-$(PCL_{20})_5$ aggregates exhibited a pH-responsive behavior. The release studies were conducted under physiological conditions (PBS, pH 7.0) and in a mildly acidic environment (PBS, pH 5.5), as illustrated in **Figure** 7. The findings indicate a notable variation in catechin release depending on the pH level. At pH 7.5, the P4VP-$(PCL_{20})_5$ aggregates maintained a compact structure, which restricted catechin diffusion. After 30 h, the cumulative release reached approximately 21%, suggesting that a significant portion of the catechin remained encapsulated within the vesicular core. Conversely, at pH 5.5, catechin release was considerably accelerated, with 39% released within 5 h and almost 80% after 24 h, demonstrating a pH-dependent controlled release without an initial burst effect. This behavior can be attributed to the increased protonation of 4VP units in P4VP-$(PCL_{20})_5$ at lower pH, which destabilizes the aggregate structure. In addition, the higher electrostatic repulsion between protonated units, due to an increased surface charge density, leads to a loosening of the vesicular network, facilitating catechin release.[50] Overall, these results confirm that polymeric vesicles can efficiently encapsulate and protect catechin at pH 7.0, while enabling targeted release at pH 5.5, demonstrating a well-regulated pH-sensitive drug delivery system.[69]

3.7. Evaluation of the functional antioxidant activity of catechin using the DPPH assay

This study evaluated the functional antioxidant activity of catechin encapsulated within polymeric aggregates, with particular focus on the long-term stability and efficacy of encapsulated catechin. The antioxidant capacity was assessed using the DPPH radical scavenging assay, comparing free catechin and encapsulated catechin. The results (**Figure 8**) revealed a significant enhancement in antioxidant performance when catechin was encapsulated. In the first stage (0–8 days), encapsulated catechin exhibited an initial activity of approximately 98%, which remained remarkably stable (>96%) throughout this period. Whereas free catechin underwent rapid degradation, dropping to only 10.9% within eight days. In the second stage (8–15 days), the antioxidant activity of encapsulated catechin decreased slightly, from 96% to 94%, confirming its long-term stability. In contrast, the antioxidant activity of free catechin remained at a very low level (6.5%). These findings highlight the crucial role of polymer-based encapsulation in protecting catechin from degradation. The improved performance is attributed to several key factors: the polymeric matrix acts as a protective barrier against environmental stressors, such as oxygen, light, and heat, known to accelerate antioxidant degradation. The encapsulation system enables sustained and controlled

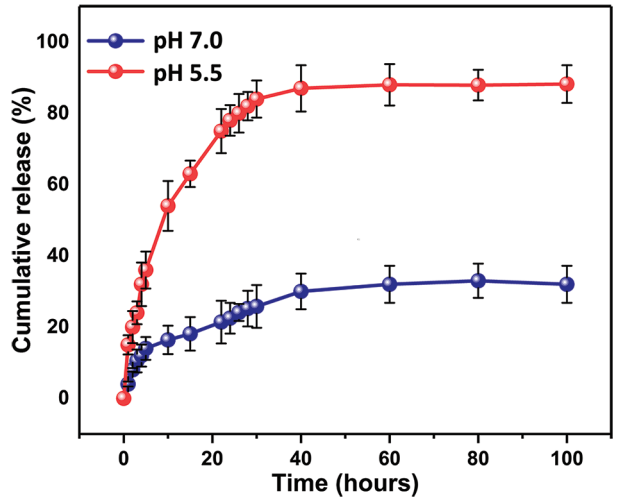

Figure 7. *In vitro* release profile of catechin from P4VP-$(PCL_{20})_5$ aggregates at pH 5.5and 7.0. Abbreviation: P4VP-$(PCL_{20})_5$: Poly(4-vinylpyridine)-(poly[ε-caprolactone]$_{20}$)$_5$

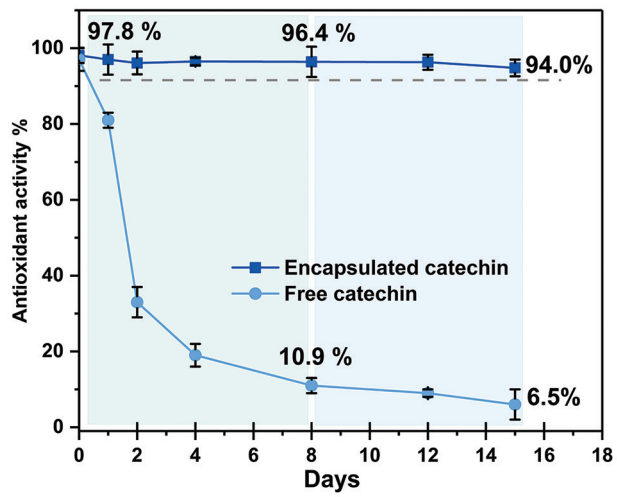

Figure 8. Evaluation of the functional antioxidant stability

release of catechin, maintaining its functional activity over an extended period, which also enhances catechin's bioavailability by improving its solubility and facilitating cellular uptake.

3.8. Improved antibacterial activity of catechin encapsulated in pH-responsive poly(4-vinylpyridine)-(poly[ε-caprolactone]$_{20}$)$_5$ vesicles

The antibacterial assays (**Figure 9A and 9B**) highlight a marked increase in efficacy after encapsulation: free catechin produces only small inhibition zones (7–8 mm, in some cases undetectable depending on the strain), while blank vesicles induce only marginal effects (7–9 mm), confirming that the activity originates from catechin itself. In contrast, encapsulation within P4VP-$(PCL_{20})_5$ vesicles substantially increases inhibition diameters at pH 5.5, typically reaching 16–19 mm for the "Cat-polymer (0.4)" formulation and up to 20–23 mm for the higher-loaded "Cat-polymer (0.6)" formulation. This dose-dependent gain (0.6 > 0.4) is consistent across all tested strains (Gram-positive and Gram-negative), with a particularly pronounced advantage for Gram-positive species (*S. aureus, Listeria monocytogenes*), while still achieving significant improvement for Gram-negative species (*E. coli, P. aeruginosa, Salmonella enterica*) despite their outer membrane barrier.

The role of pH is critical; at pH 5.5, the pyridyl units of P4VP become protonated, increasing the hydrophilicity of the segment, inducing swelling/disorganization of the vesicles, and accelerating catechin release. This spatiotemporal release results in a locally elevated concentration in proximity to bacterial cells, enhancing the diffusion gradient across the cell envelope. Simultaneously, the protection provided by the hydrophobic PCL core and the multilayer vesicular architecture reduces catechin oxidation and enzymatic degradation before the vesicles reach the target, increasing the fraction of active molecules available. The increase in surface charge (zeta potential) at pH 5–6 (due to P4VP protonation) may also promote electrostatic interactions with the overall negatively charged bacterial surfaces, facilitating vesicle adhesion and local drug delivery. The pH 7 versus pH 5.5 comparison confirms the pH-triggered nature of the system: at neutral pH, inhibition zones remain modest (10–13 mm), whereas at pH 5.5, they sharply increase (18–23 mm), consistent with accelerated release kinetics under acidic conditions. This trend is reflected in the minimum inhibitory concentration (MIC) values (pH 5.5), which are significantly lower for the encapsulated formulations compared to free catechin, corroborating the pharmacodynamic superiority imparted by vectorization.

Figure 9C shows that, for all five tested bacterial strains (*E. coli*, *S. enterica*, *L. monocytogenes*, *P. aeruginosa*, and *S. aureus*), the MIC values of catechin encapsulated in P4VP-$(PCL_{20})_5$ vesicles "Cat-polymer (0.4)" and "Cat-polymer (0.6)" at pH 5.5 were dramatically reduced compared to those of free catechin. This reduction was consistent across all tested bacterial strains, with decreases of up to 10–20-fold, confirming that the encapsulation system enables targeted and efficient release in acidic environments. In comparison with literature data, free catechin typically exhibits MICs of 1–2 mg/mL against *S. aureus* and *E. coli*.[70,71] In our study, MICs for the encapsulated forms dropped below 100 μg/mL for most strains, demonstrating a significant gain in efficacy. This improvement can be attributed to the protection of catechin from enzymatic and oxidative degradation due to the multilayer vesicular structure, the pH-responsiveness of the P4VP block, which drives vesicle disassembly and targeted release in the acidic microenvironment of infectious sites (pH 5.5), and improved local bioavailability, enabling bactericidal concentrations to be reached more rapidly and at lower doses.

These findings align with other studies showing that encapsulation of polyphenols or antimicrobial agents in pH-sensitive nanostructures can significantly enhance activity against both Gram-positive and Gram-negative pathogens.[72]

4. Limitations and future perspectives

Although this study provides valuable insights into polymer-based drug delivery systems, it is limited to laboratory-scale design, which does not fully replicate the complexity of

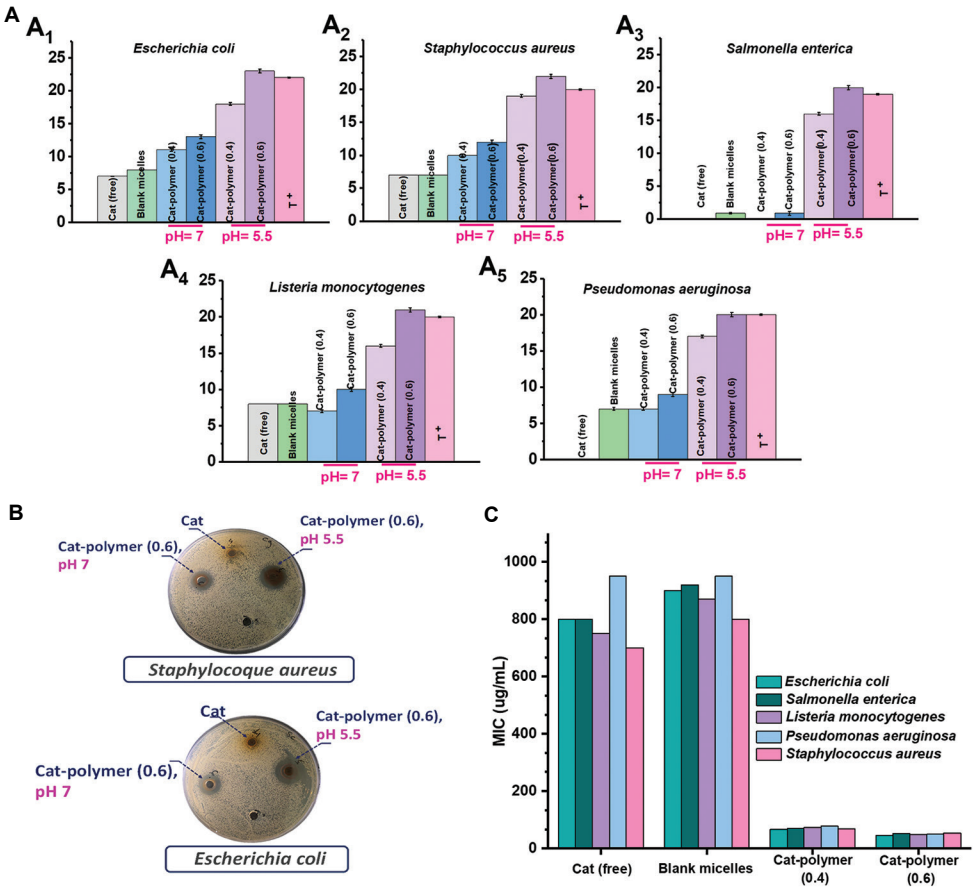

Figure 9. Antibacterial activity and pH-dependent MIC reduction of catechin encapsulated in P4VP-$(PCL_{20})_5$ vesicles. (A) Inhibition zones for different microbes at pH 7 and pH 5.5. (B) Inhibition zones for *Escherichia coli* and *Staphylococcus aureus* at pH 7 and pH 5.5. (C) MIC values for free catechin and encapsulated catechin at pH 5.5.
Abbreviations: Cat: Catechin; MIC: Minimum inhibitory concentration; P4VP-$(PCL_{20})_5$: Poly(4-vinylpyridine)$_{50}$-(poly[ε-caprolactone]$_{20}$)$_5$; T: Gentamicin.

physiological environments. In addition, long-term stability, degradation, and potential biological effects require further evaluation.

Looking forward, future work should focus on *in vitro* and *in vivo* biocompatibility, pharmacokinetics, and targeted efficacy, as well as scaling up the synthesis process and testing under realistic conditions. Exploring advanced polymer architectures, investigating stimuli-responsive systems, and integrating computational modeling could further optimize drug encapsulation and release, paving the way for practical applications.

5. Conclusions

The present study demonstrates that the amphiphilic copolymer P4VP-$(PCL_{20})_5$ forms highly pH-sensitive multilamellar vesicles capable of efficiently encapsulating catechin. Upon self-assembly in aqueous media, the copolymer generated stable nanostructures with diameters ranging from 90 to 130 nm, as confirmed by DLS and TEM. Physicochemical characterization revealed a sharp solubility transition around pH 5.5, attributed to the protonation of the tertiary amine groups of P4VP. This transition was marked by an increase in vesicle size, a rise in zeta potential (+42 mV), and a significant drop in transmittance (< 1%), indicating vesicle destabilization and partial precipitation of the copolymer.

Encapsulation of catechin within these vesicles led to a significant enhancement of its stability, antioxidant activity, and bioavailability. The release of catechin was shown to be strongly pH-dependent: at physiological pH (7.0), the vesicles remained structurally stable, allowing limited release (<10% over 24 h); whereas at acidic pH (5.5), which is the characteristic of infection-related microenvironments, protonation induced disassembly of the vesicles and triggered rapid release of the active compound (> 90% in 24 h; > 50% in 4 h). This selective release behavior translated into potent antibacterial activity, particularly against acidifying pathogens. Inhibition zones reached 23 mm for *E. coli*, 22 mm for *S. aureus*, 20 mm for *P. aeruginosa*, and 21 mm for *L. monocytogenes* at pH 5.5.

In contrast, free catechin exhibited significantly lower antibacterial activity under the same conditions, with inhibition diameters not exceeding 8 mm. This highlights the crucial role of encapsulation in enhancing the therapeutic efficacy of catechin. The improved antibacterial performance can be attributed to several synergistic factors: (i) protection of catechin against enzymatic and oxidative degradation, (ii) enhanced interactions with bacterial membranes mediated by the positive charge of

protonated P4VP, and (iii) controlled release leading to optimal local concentrations at the infection site.

In addition to its antimicrobial effects, the vesicular system also conferred prolonged antioxidant activity to catechin, as evidenced by DPPH radical scavenging assays. The encapsulated catechin retained its antioxidant potential over extended periods, whereas the free form showed rapid degradation. This indicated that the copolymer matrix provided an effective barrier against oxidative stress, thereby prolonging the functional lifespan of the bioactive compound.

Overall, this study not only introduces a novel pH-responsive delivery platform for catechin but also opens new perspectives for the development of targeted antimicrobial therapies. The use of multi-branched P4VP-$(PCL_{20})_5$ copolymer vesicles could be extended to the encapsulation of other bioactive molecules, thereby broadening their potential applications in combating a wide range of bacterial infections, particularly those caused by MDR strains. Such systems could also be tailored for site-specific drug release in other pathological conditions characterized by pH variations, such as cancer or inflammatory diseases. Nevertheless, some limitations should be acknowledged, including the need for further *in vivo* evaluation to confirm therapeutic efficacy and safety, as well as the optimization of large-scale production methods to ensure reproducibility and cost-effectiveness. Addressing these aspects will be essential for translating this strategy into clinical applications.

Acknowledgement
None.
Financial support
None.
Conflicts of interest statement
The researchers declare that they do not have any conflicts of interest concerning this publication.
Author contributions
Conceptualization: MB; *Data curation*: MB and MD; *Formal analysis*: OS and AH; *Writing – original draft:* MB; *Writing – review & editing:* REY, AH, and AM. All authors read and approved the final manuscript.
Ethics approval and consent to participate
Not applicable.
Consent for publication
Not applicable.
Availability of data
No datasets were generated or analyzed during the current study.

References

1. Medina E, Pieper DH. Tackling threats and future problems of multidrug-resistant bacteria. In: *How to Overcome the Antibiotic Crisis: Facts, Challenges, Technologies and Future Perspectives*. Berlin: Springer; 2016. p. 3-33.
2. Alara JA, Alara OR. An overview of the global alarming increase of multiple drug resistant: A major challenge in clinical diagnosis. *Infect Disord Drug Targets*. 2024;24(3):26-42. doi: 10.2174/1871526523666230725103902
3. Yu Q, Wang C, Zhang X, Chen H, Wu MX, Lu M. Photochemical strategies toward precision targeting against multidrug-resistant bacterial infections. *ACS Nano*. 2024;18(22):14085-14122. doi: 10.1021/acsnano.3c12714
4. Huang YC, Kuo SC, Fang CT, Lauderdale TL. Changing epidemiology and antimicrobial resistance of bacteria causing bacteremia in Taiwan: 2002-2020. *Microbiol Spectr*. 2024;12(8):e0060824. doi: 10.1128/spectrum.00608-24
5. Adouane M, Kadri N, Benzitoune N, *et al*. Understanding bacterial diversity, infection dynamics, prevention of antibiotic resistance: An integrated study in an Algerian hospital context. *Eur J Clin Microbiol Infect Dis*. 2024;43(11):2093-2105. doi: 10.1007/s10096-024-04919-3
6. Sadones O, Kramarska E, Laverde D, Berisio R, Huebner J, Romero-Saavedra F. Investigation of cross-opsonic effect leads to the discovery of PPIase-domain containing protein vaccine candidate to prevent infections by Gram-positive ESKAPE pathogens. *BMC Microbiol*. 2024;24(1):280. doi: 10.1186/s12866-024-03427-w
7. Shafique S, Jabeen N, Irum S, Mehmood A, Ahmad KS. Expression of mastitis causing fibrinogen binding protein of gram positive bacteria in genetically engineered switchgrass and antibodies production in mice. *Physiol Mol Biol Plants*. 2024;30(11):1829-1839. doi: 10.1007/s12298-024-01528-4
8. Bisola MAI, Olatunji G, Kokori E, *et al*. Emerging challenges in innate immunity: *Staphylococcus aureus* and healthcare-associated infection. *J Med Surg Public Health*. 2024;3:100103. doi: 10.1016/j.glmedi.2024.100103
9. Goormaghtigh F, Van Bambeke F. Understanding *Staphylococcus aureus* internalisation and induction of antimicrobial tolerance. *Exp Rev Anti Infect Ther*. 2024;22(1-3):87-101. doi: 10.1080/14787210.2024.2303018
10. Zeferino AS, Mira AR, Delgadinho M, Brito M, Ponte T, Ribeiro E. Drug resistance and epigenetic modulatory potential of epigallocatechin-3-gallate against *Staphylococcus aureus*. *Curr Microbiol*. 2022;79(5):149. doi: 10.1007/s00284-022-02841-5
11. Liang Z, Liu W, Wang Z, *et al*. Near-infrared laser-controlled nitric oxide-releasing gold nanostar/hollow polydopamine Janus nanoparticles for synergistic elimination of methicillin-resistant *Staphylococcus aureus* and wound healing. *Acta Biomater*. 2022;143:428-444. doi: 10.1016/j.actbio.2022.02.029
12. Veiko AG, Olchowik-Grabarek E, Sekowski S, *et al*. Antimicrobial activity of quercetin, naringenin and catechin: Flavonoids inhibit *Staphylococcus aureus*-induced hemolysis and modify membranes of bacteria and erythrocytes. *Molecules*. 2023;28(3):1252. doi: 10.3390/molecules28031252
13. Renzetti A, Betts JW, Fukumoto K, Rutherford RN. Antibacterial green tea catechins from a molecular perspective: Mechanisms of action and structure-activity relationships. *Food Funct*. 2020;11(11):9370-9396. doi: 10.1039/d0fo02054k
14. Bae J, Kim N, Shin Y, Kim SY, Kim YJ. Activity of catechins and their applications. *Biomed Dermatol*. 2020;4:1-10.
15. Gadkari PV, Balaraman M. Catechins: Sources, extraction and encapsulation: A review. *Food Bioprod Process*. 2015;93:122-138. doi: 10.1016/j.fbp.2013.12.004
16. Parisi OI, Puoci F, Restuccia D, Farina G, Iemma F, Picci N. Polyphenols and their formulations: Different strategies to overcome the drawbacks associated with their poor stability and bioavailability. In: *Polyphenols in Human Health and Disease*. Netherlands: Elsevier; 2014. p. 29-45.
17. Alfei S, Schito AM, Zuccari G. Nanotechnological manipulation of nutraceuticals and phytochemicals for healthy purposes: Established advantages vs. Still undefined risks. *Polymers (Basel)*. 2021;13(14):2262. doi: 10.3390/polym13142262
18. Ahmad SR, Ghosh P. A systematic investigation on flavonoids, catechin, β-sitosterol and lignin glycosides from *Saraca asoca* (ashoka) having anti-cancer & antioxidant properties with no side effect. *J Indian Chem Soc*. 2022;99(1):100293. doi: 10.1016/j.jics.2021.100293
19. Mani JS, Johnson JB, Hosking H, *et al*. Antioxidative and therapeutic potential of selected Australian plants: A review. *J Ethnopharmacol*. 2021;268:113580. doi: 10.1016/j.jep.2020.113580

20. Sultana A, Zare M, Thomas V, Kumar TS, Ramakrishna S. Nano-based drug delivery systems: Conventional drug delivery routes, recent developments and future prospects. *Med Drug Discov.* 2022;15:100134. doi: 10.1016/j.medidd.2022.100134
21. Wu M, Brown AC. Applications of catechins in the treatment of bacterial infections. *Pathogens.* 2021;10(5):546. doi: 10.3390/pathogens10050546
22. Fathima A, Rao JR. Selective toxicity of catechin-a natural flavonoid towards bacteria. *Appl Microbiol Biotechnol.* 2016;100:6395-6402. doi: 10.1007/s00253-016-7492-x
23. Sharma A, Gupta VK, Pathania R. Efflux pump inhibitors for bacterial pathogens: From bench to bedside. *Indian J Med Res.* 2019;149(2):129-145. doi: 10.4103/ijmr.IJMR_2079_17
24. Miklasińska-Majdanik M, Kępa M, Wojtyczka RD, Idzik D, Wąsik TJ. Phenolic compounds diminish antibiotic resistance of *Staphylococcus aureus* clinical strains. *Int J Environ Res Public Health.* 2018;15(10):2321. doi: 10.3390/ijerph15102321
25. Álvarez-Martínez FJ, Barrajón-Catalán E, Encinar JA, Rodríguez-Díaz JC, Micol V. Antimicrobial capacity of plant polyphenols against gram-positive bacteria: A comprehensive review. *Curr Med Chem.* 2020;27(15):2576-2606. doi: 10.2174/0929867325666181008115650
26. Murugan S, Senthilvelan T, Govindasamy M, Thangavel K. A comprehensive review on exploring the potential of phytochemicals and biogenic nanoparticles for the treatment of antimicrobial-resistant pathogenic bacteria. *Curr Microbiol.* 2025;82(2):90. doi: 10.1007/s00284-025-04064-w
27. Liu H, Song P, Zhang H, *et al.* Synthetic biology-based bacterial extracellular vesicles displaying BMP-2 and CXCR4 to ameliorate osteoporosis. *J Extracell Vesicles.* 2024;13(4):e12429. doi: 10.1002/jev2.12429
28. Liu H, Zhang Q, Wang S, Weng W, Jing Y, Su J. Bacterial extracellular vesicles as bioactive nanocarriers for drug delivery: Advances and perspectives. *Bioact Mater.* 2022;14:169-181. doi: 10.1016/j.bioactmat.2021.12.006
29. Chiabotto G, Semnani A, Ceccotti E, Bruno S. Extracellular vesicles: Emerging therapeutic agents for liver fibrosis. *Extracell Vesicles Circ Nucl Acids.* 2025;6(2):216-244. doi: 10.20517/evcna.2025.08
30. Wang F, Li Z. Engineered extracellular vesicles as "supply vehicles" to alleviate type 1 diabetes. *Extracell Vesicles Circ Nucl Acids.* 2024;5(4):618-621. doi: 10.20517/evcna.2024.61
31. Qi C, Liu G, Ping Y, *et al.* A comprehensive review of nano-delivery system for tea polyphenols: Construction, applications, and challenges. *Food Chem X.* 2023;17:100571. doi: 10.1016/j.fochx.2023.100571
32. Shikha D, Singh A, Rangra NK, Monga V, Bhatia R. Insights to therapeutic potentials, pharmaceutical formulations, chemistry and analytical methods of catechin. *Phytochem Rev.* 2024;23:1557-1598. doi: 10.1007/s11101-024-09929-9
33. Wang X, Fan Y, Yan J, Yang M. Engineering polyphenol-based polymeric nanoparticles for drug delivery and bioimaging. *Chem Eng J.* 2022;439:135661. doi: 10.1016/j.cej.2022.135661
34. Vittorio O, Curcio M, Cojoc M, *et al.* Polyphenols delivery by polymeric materials: Challenges in cancer treatment. *Drug Deliv.* 2017;24(1):162-180. doi: 10.1080/10717544.2016.1236846
35. Zhang R, Ma Q, Zheng N, *et al.* Plant polyphenol-based injectable hydrogels: Advances and biomedical applications. *Adv Healthc Mater.* 2025;14(12):2500445. doi: 10.1002/adhm.202500445
36. Xu C, Zhou S, Song H, *et al.* Green tea polyphenols-derived hybrid materials in manufacturing, environment, food and healthcare. *Nano Today.* 2023;52:101990. doi: 10.1016/j.nantod.2023.101990
37. Pecorini G, Ferraro E, Puppi D. Polymeric systems for the controlled release of flavonoids. *Pharmaceutics.* 2023;15(2):628. doi: 10.3390/pharmaceutics15020628
38. Pidwill GR, Gibson JF, Cole J, Renshaw SA, Foster SJ. The role of macrophages in *Staphylococcus aureus* infection. *Front Immunol.* 2021;11:620339. doi: 10.3389/fimmu.2020.620339
39. Flannagan RS, Kuiack RC, McGavin MJ, Heinrichs DE. *Staphylococcus aureus* uses the GraXRS regulatory system to sense and adapt to the acidified phagolysosome in macrophages. *MBio.* 2018;9(4):e01143-18. doi: 10.1128/mbio.01143-18
40. Flannagan RS, Heit B, Heinrichs DE. Antimicrobial mechanisms of macrophages and the immune evasion strategies of *Staphylococcus aureus*. *Pathogens.* 2015;4(4):826-868. doi: 10.3390/pathogens4040826
41. Rasquel-Oliveira FS, Ribeiro JM, Martelossi-Cebinelli G, *et al.* *Staphylococcus aureus* in inflammation and pain: Update on pathologic mechanisms. *Pathogens.* 2025;14(2):185. doi: 10.3390/pathogens14020185
42. Leonarduzzi G, Testa G, Sottero B, Gamba P, Poli G. Design and development of nanovehicle-based delivery systems for preventive or therapeutic supplementation with flavonoids. *Curr Med Chem.* 2010;17(1):74-95. doi: 10.2174/092986710789957760
43. Elkhalifa ME, Ashraf M, Ahmed A, *et al.* Polyphenols and their nanoformulations as potential antibiofilm agents against multidrug-resistant pathogens. *Future Microbiol.* 2024;19(3):255-279. doi: 10.2217/fmb-2023-0175
44. Shahi F, Afshar H, Dawi EA, Khonakdar HA. Smart microneedles in biomedical engineering: Harnessing stimuli-responsive polymers for novel applications. *Polym Adv Technol.* 2024;35(12):e70020. doi: 10.1002/pat.70020
45. Zhao N, Yan L, Zhao X, *et al.* Versatile types of organic/inorganic nanohybrids: From strategic design to biomedical applications. *Chem Rev.* 2018;119(3):1666-1762. doi: 10.1021/acs.chemrev.8b00401
46. Pisoschi AM, Pop A, Cimpeanu C, Turcuş V, Pre doi G, Iordache F. Nanoencapsulation techniques for compounds and products with antioxidant and antimicrobial activity-A critical view. *Eur J Med Chem.* 2018;157:1326-1345. doi: 10.1016/j.ejmech.2018.08.076
47. Mukurumbira A, Shellie RA, Keast R, Palombo EA, Jadhav SR. Encapsulation of essential oils and their application in antimicrobial active packaging. *Food Control.* 2022;136:108883. doi: 10.1016/j.foodcont.2022.108883
48. Ben-Fadhel Y, Maherani B, Manus J, Salmieri S, Lacroix M. Physicochemical and microbiological characterization of pectin-based gelled emulsions coating applied on pre-cut carrots. *Food Hydrocolloids.* 2020;101:105573. doi: 10.1016/j.foodhyd.2019.105573
49. Guerra-Rosas MI, Morales-Castro J, Cubero-Márquez MA, Salvia-Trujillo L, Martín-Belloso O. Antimicrobial activity of nanoemulsions containing essential oils and high methoxyl pectin during long-term storage. *Food Control.* 2017;77:131-138. doi: 10.1016/j.foodcont.2017.02.008
50. Sabaghi M, Hoseyni SZ, Tavasoli S, Mozafari M, Katouzian I. Strategies of confining green tea catechin compounds in nano-biopolymeric matrices: A review. *Colloids Surf B Biointerfaces.* 2021;204:111781. doi: 10.1016/j.colsurfb.2021.111781
51. El Yousfi R, Achalhi N, Brahmi M, *et al.* Controlled synthesis of linear and multi ARM amphiphilic copolymers consisting of P4VP and PCL for tailored nano-aggregate formation. *J Mol Liquids.* 2024;394:123774. doi: 10.1016/j.molliq.2023.123774
52. Yousfi RE, Atanase LI, Makaoui A, *et al.* Enhanced quercetin encapsulation through charge density and amphiphilicity tuning in cationic triblock micelles. *ACS Appl Polym Mater.* 2025;7:6365-6383. doi: 10.1021/acsapm.5c00806
53. Gröschel AH, Müller AH. Self-assembly concepts for multicompartment nanostructures. *Nanoscale.* 2015;7(28):11841-11876. doi: 10.1039/C5NR02448J
54. Brisson ER, Worthington MJ, Kerai S, Müllner M. Nanoscale polymer discs, toroids and platelets: A survey of their syntheses and potential applications. *Chem Soc Rev.* 2024;53(4):1984-2021.

doi: 10.1039/D1CS01114F
55. Brand-Williams W, Cuvelier ME, Berset C. Use of a free radical method to evaluate antioxidant activity. *LWT Food Sci Technol.* 1995;28(1):25-30. doi: 10.1016/S0023-6438(95)80008-5
56. Wu KH, Wang YR, Hwu WH. FTIR and TGA studies of poly(4-vinylpyridine-co-divinylbenzene)-Cu (II) complex. *Polym Degrad Stabil.* 2003;79(2):195-200. doi: 10.1016/S0141-3910(02)00261-6
57. Elzein T, Nasser-Eddine M, Delaite C, Bistac S, Dumas P. FTIR study of polycaprolactone chain organization at interfaces. *J Colloid Interface Sci.* 2004;273(2):381-387. doi: 10.1016/j.jcis.2004.02.001
58. Liu H, Ding M, Ding Z, Gao C, Zhang W. *In situ* synthesis of the Ag/poly(4-vinylpyridine)-block-polystyrene composite nanoparticles by dispersion RAFT polymerization. *Polym Chem.* 2017;8(20):3203-3210. doi: 10.1039/C7PY00473G
59. Ferrari R, Yu Y, Morbidelli M, Hutchinson RA, Moscatelli D. ε-Caprolactone-based macromonomers suitable for biodegradable nanoparticles synthesis through free radical polymerization. *Macromolecules.* 2011;44(23):9205-9212. doi: 10.1021/ma201955p
60. Sahiner N, Ozay O. Responsive tunable colloidal soft materials based on p (4-VP) for potential biomedical and environmental applications. *Colloids Surfaces A Physicochem Eng Aspects.* 2011;378(1-3):50-59. doi: 10.1016/j.colsurfa.2011.01.053
61. Sahiner N, Yasar AO. The generation of desired functional groups on poly (4-vinyl pyridine) particles by post-modification technique for antimicrobial and environmental applications. *J Colloid Interface Sci.* 2013;402:327-333. doi: 10.1016/j.jcis.2013.03.032
62. Amalvy J, Wanless E, Li Y, Michailidou V, Armes S, Duccini Y. Synthesis and characterization of novel pH-responsive microgels based on tertiary amine methacrylates. *Langmuir.* 2004;20(21):8992-8999. doi: 10.1021/la049156t
63. Li Y, Gao GH, Lee DS. Stimulus-sensitive polymeric nanoparticles and their applications as drug and gene carriers. *Adv Healthc Mater.* 2013;2(3):388-417. doi: 10.1002/adhm.201200313
64. Ding H, Tan P, Fu S, *et al.* Preparation and application of pH-responsive drug delivery systems. *J Control Release.* 2022;348:206-238. doi: 10.1016/j.jconrel.2022.05.056
65. He X, Li J, An S, Jiang C. pH-sensitive drug-delivery systems for tumor targeting. *Ther Deliv.* 2013;4(12):1499-1510. doi: 10.4155/tde.13.120
66. Mendrek S, Mendrek A, Adler HJ, Dworak A, Kuckling D. Synthesis and characterization of pH sensitive poly (glycidol)-b-poly (4-vinylpyridine) block copolymers. *J Polym Sci Part A Polym Chem.* 2009;47(7):1782-1794. doi: 10.1002/pola.23276
67. Sahiner N, Atta AM, Yasar AO, Al-Lohedan HA, Ezzat AO. Surface activity of amphiphilic cationic pH-responsive poly(4-vinylpyridine) microgel at air/water interface. *Colloids Surf A Physicochem Eng Aspects.* 2015;482:647-655. doi: 10.1016/j.colsurfa.2015.07.035
68. Mishra AK, Lim J, Lee J, *et al.* Control drug release behavior by highly stable and pH sensitive poly (N-vinylpyrrolidone)-block-poly (4-vinylpyridine) copolymer micelles. *Polymer.* 2021;213:123329. doi: 10.1016/j.polymer.2020.123329
69. Aljuffali IA, Lin CH, Yang SC, Alalaiwe A, Fang JY. Nanoencapsulation of tea catechins for enhancing skin absorption and therapeutic efficacy. *Aaps PharmSciTech.* 2022;23(6):187. doi: 10.1208/s12249-022-02344-3
70. Kono K, Tatara I, Takeda S, Arakawa K, Hara Y. Antibacterial activity of epigallocatechin gallate against methicillin-resistant *Staphylococcus aureus. Kansenshogaku Zasshi.* 1994;68(12):1518-1522. doi: 10.11150/kansenshogakuzasshi1970.68.1518
71. Miklasińska M, Kępa M, Wojtyczka RD, Idzik D, Dziedzic A, Wąsik TJ. Catechin hydrate augments the antibacterial action of selected antibiotics against *Staphylococcus aureus* clinical strains. *Molecules.* 2016;21(2):244. doi: 10.3390/molecules21020244
72. Liu S, Zhang Q, Li H, Qiu Z, Yu Y. Comparative assessment of the antibacterial efficacies and mechanisms of different tea extracts. *Foods.* 2022;11(4):620. doi: 10.3390/foods11040620

Received: June 10, 2025
Revised: August 25, 2025
Accepted: August 28, 2025
Available online: November 14, 2025